7930 *Biochemistry* **2010,** *49,* 7930–7938
DOI: 10.1021/bi100894r

BIOCHEMISTRY
including biophysical chemistry & molecular biology
Article

Evidence of Adaptability in Metal Coordination Geometry and Active-Site Loop Conformation among B1 Metallo-β-lactamases[†,‡]

Javier M. González,[§,⊥] Alejandro Buschiazzo,*[,∥] and Alejandro J. Vila*[,§]

[§]*Instituto de Biología Molecular y Celular de Rosario (IBR), Consejo Nacional de Investigaciones Científicas y Técnicas (CONICET), Facultad de Ciencias Bioquímicas y Farmacéuticas, Universidad Nacional de Rosario (UNR), Suipacha 531, S2002LRK Rosario, Argentina, and* [∥]*Institut Pasteur de Montevideo, Unidad de Cristalografía de Proteínas, Mataojo 2020, 11400 Montevideo, Uruguay, and Institut Pasteur, Department of Structural Biology and Chemistry, 25 rue du Dr Roux, 75015 Paris, France*
[⊥]*Current address: Department of Pharmaceutical Sciences and UMXSS Crystallography Service, University of Maryland, Baltimore, MD 21201.*

Received June 3, 2010; Revised Manuscript Received July 29, 2010

ABSTRACT: Subclass B1 β-lactamases are Zn(II)-dependent hydrolases that confer bacterial resistance to most clinically useful β-lactam antibiotics. The enzyme BcII from *Bacillus cereus* is a prototypical enzyme that belongs to this group, the first Zn(II)-dependent β-lactamase to be discovered. Crucial aspects of the BcII catalytic mechanism and metal binding mode have been assessed mostly on the Co(II)-substituted surrogate. Here we report a high-resolution structure of Co(II)-BcII, revealing a metal coordination geometry identical to that of the native zinc enzyme. In addition, a high-resolution structure of the apoenzyme, together with structures with different degrees of metal occupancy and oxidation levels of a conserved Cys ligand, discloses a considerable mobility of two loops containing four metal ligands (namely, regions His116−Arg121 and Gly219−Cys221). This flexibility is expected to assist in the structural rearrangement of the metal sites during catalytic turnover, which, along with the coordination geometry adaptability of Zn(II) ions, grants the interaction with a variety of substrates, a characteristic feature of B1 metallo-β-lactamases.

Bacterial resistance to antibiotics remains a major issue in the clinical setting despite the continuous development of new antimicrobial compounds (*1*, *2*). β-Lactam antibiotics are the most commonly prescribed drugs for treatment of bacterial infections and are targeted by a number of resistance mechanisms, among which the production of β-lactamases is the most effective. These enzymes are able to inactivate β-lactams by hydrolyzing their cyclic amide (*3*, *4*). Metallo-β-lactamases (MβLs)[1] represent the newest generation of broad-spectrum β-lactamases, active on virtually all clinically useful β-lactam antibiotics. MβLs are zinc-dependent enzymes able to hydrolyze penicillins, cephalosporins, and carbapenems, being insensitive to inhibitors of nonmetallic β-lactamases (*5*, *6*). The lack of a clinically useful inhibitor is mostly due to the structural diversity of active sites amid MβLs from different sources, regarding features like metal content, metal coordinating residues, and accessibility of the drug to the active site. On the basis of this diversity, MβLs have been further grouped into three subclasses: B1, B2, and B3 (*7*). B1 enzymes are the most bothersome at the clinical level, often encoded in mobile genetic elements subject to horizontal gene transfer and selection for improved catalytic properties (*1*, *2*), like IMP-, VIM-, GIM-, and SPM-type lactamases (*8*).

The MβL from *Bacillus cereus*, BcII, is a prototypical B1 enzyme whose three-dimensional structure was determined in 1995, revealing a characteristic αβ/βα fold and a metal-binding motif (*9*), HXHXDX, currently regarded as the hallmark of the metallo-β-lactamase superfamily (*8*, *10*). The active site is located at the bottom of a solvent-accessible crevice, delimited by several loops (Figure 1). Two of them flank the active site: loop L10, harboring residues Lys224 and Asn233, both implicated in substrate binding (*11*−*14*), as well as residue Cys221, a key Zn(II) ligand conserved in B1 and B2 enzymes; and loop L3, enclosing aromatic residues such as Phe64 that come into contact with the substrate upon binding (*15*, *16*). The floor of the active site is defined by loop L7, which includes residues His116−Arg121 in the aforementioned metal-binding motif; as well as loops L9 and L12, containing metal-liganding residues His196 and His263, respectively.

BcII can bind up to two Zn(II) ions, in the so-called 3H and DCH sites, with metal-binding residues His116, His118, and His196 and metal-binding residues Asp120, Cys221, and His263,

[†]This work has been supported by grants from HHMI (Howard Hughes Medical Institute), CONICET (Consejo Nacional de Investigaciones Científicas y Técnicas), and ANPCyT (Agencia Nacional de Promoción Científica y Tecnológica) to A.J.V. and a fellowship from Programa AMSUD-Pasteur to J.M.G. A.B. acknowledges support from IP-Montevideo. All authors acknowledge support from CeBEM (CNPq-PROSUL). A.J.V. is a fellow of the John Simon Guggenheim Foundation.

[‡]Atomic coordinates and structure factors have been deposited in the Protein Data Bank as entries 3i15 (BcII-Ocs), 3i0v (BcII-Apo), 3i13 (BcII-diZn), 3i11 (BcII-diCo), and 3i14 (BcII-Gol).

*To whom correspondence should be addressed. A.J.V.: e-mail, vila@ibr.gov.ar; phone, +54-3414350661, ext. 108; fax, +54-341-4390465. A.B.: e-mail, alebus@pasteur.edu.uy; phone, +598-25220910, ext. 120; fax, +598-25224185.

[1]Abbreviations: ML, mother liquor; PEG, polyethylene glycol; DTT, dithiothreitol; Ocs, cysteine sulfonate residue; TCEP, tris(2-carboxyethyl)phosphine; MβL, metallo-β-lactamase; BCT, bicarbonate; CIT, citrate; Gol, glycerol; BcII-Ocs, structure of BcII with residue Cys221 oxidized; BcII-Apo, structure of the apoprotein; BcII-diZn, structure of BcII bound to two Zn(II) atoms; BcII-diCo, structure of BcII bound to two Co(II) atoms; BcII-Gol, structure of BcII-di-Co with residue Cys221 partially oxidized; HAHADR, Ala119−Arg121 loop; GGC, Gly219−Cys221 loop; PDB, Protein Data Bank; rmsd, root-mean-square deviation.

 Published on Web 08/02/2010

respectively (Figure 2). The crystal structure of BcII (PDB entry 1bmc) (*9*), the first MβL to be disclosed, revealed the presence of a single Zn(II) ion in the 3H site (Figure 2a). In contrast, a subsequent structure, that of CcrA MβL from *Bacteroides fragilis* (PDB entry 1znb), showed two Zn(II) ions in the active site: Zn1 and Zn2 in the 3H and DCH sites, respectively (*17*). This led to the hypothesis that BcII was a mononuclear Zn(II) enzyme. However, spectroscopic studies performed on Co(II)-substituted BcII allowed us to demonstrate the presence of a second metal-binding site (*18*). Indeed, crystal structures of BcII harboring both Zn(II) ions were actually reported afterward (PDB entries 1bc2 and 1bvt) (*19*, *20*), showing that the second Zn(II) site in BcII is equivalent to the Zn2 site in CcrA (Figure 2b,c). The structure of dinuclear BcII determined at pH 4.5 (PDB entry 1bc2) displays a Zn1 site in a distorted tetrahedral geometry, bound to three His residues and a nucleophilic water/OH^- molecule, located 2.48 Å (chain A) and 3.06 Å (chain B) from Zn2. Instead, Zn2 exhibits a trigonal-bipyramidal geometry, with three equatorial ligands (Cys221 Sγ, His263 Nε2, and the nucleophile), and Asp120 Oδ1 and a second water molecule in the two axial positions (Figure 2b). In the structure determined at pH 5.6 (PDB entry 1bvt), the Zn1 ion shows a trigonal-bipyramidal geometry, with a water molecule at 2.09 Å occupying an axial solvent-accessible position (Figure 2c). Remarkably, this structure lacks the bridging nucleophile, despite the presence of both metal ions. The Zn2 ion exhibits a distorted trigonal-bipyramidal geometry, due to the presence of a bound bicarbonate ion (BCT).

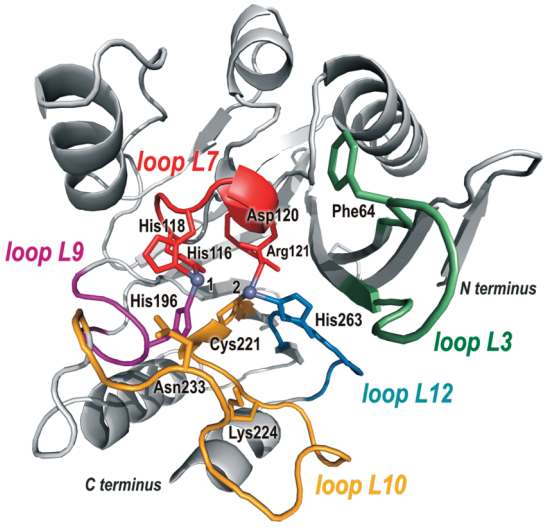

FIGURE 1: Global fold of BcII, highlighting the loop topology, based on PDB entry 1bvt. Noncovalently bound molecules have been omitted for the sake of clarity (see Figure 2c). Numbers 1 and 2 indicate the metal sites.

One of the most controversial aspects of β-lactam hydrolysis by MβLs is the role and essentiality of each metal ion (*21*−*24*). Although the availability of crystal structures of mono-Zn and di-Zn BcII suggests that the metal ions bind in a sequential manner, that is, the first Zn(II) equivalent binds to the 3H site and then the second to the DCH site, experimental evidence shows that metal binding to BcII in solution does not follow this behavior (*25*−*27*).

So far, all attempts to obtain a crystallographic structure of an MβL in complex with a native substrate have been unsuccessful. The structures of enzyme−product complexes for enzymes CphA (subclass B2) and L1 (subclass B3) have provided some clues about the mechanism (*21*, *23*). The use of spectroscopic techniques has been of great relevance for the mechanistic study of these enzymes, particularly for those of subclass B1. BcII is known to exhibit hydrolytic activity as Cd(II), Ni(II), Mn(II), and Co(II) adducts (*28*, *29*), which led to an extensive usage of metal substitution in the analysis of the active site. Because Zn(II) is a closed-shell d^{10} transition metal ion, silent to most spectroscopic techniques, high-spin Co(II) ($S = {}^3/_2$) has been applied in studying several Zn(II) sites in proteins (*30*), including MβL-catalyzed hydrolysis of β-lactams for more than 25 years (*31*−*36*). Given the ability of BcII to retain its activity upon Co(II) substitution (*18*, *27*), Co(II)-BcII is a suitable system for studying the structure and mechanism of MβLs in solution (*3*, *4*, *31*, *32*, *37*).

Recent results in the closely related B1 enzyme from *Bacillus anthracis* have shown a differential behavior in Zn(II) and Co(II) binding (*38*), which prompted a detailed reassessment of the enzyme active-site architecture upon Co(II) substitution. Furthermore, kinetic and spectroscopic data acquired for Co(II)-BcII have been interpreted considering the available crystallographic models of Zn(II)-BcII (*3*, *4*, *18*, *39*, *40*). Given the fact that no crystal structures of Co(II)-substituted MβLs are currently available, Co(II) substitution on BcII has led to controversial discussions of enzyme features contrasting crystallographic and spectroscopic evidence (*3*, *18*, *27*, *41*). Here we report the crystallographic structure of Co(II)-BcII, in an attempt to help circumvent these discrepancies. We show that BcII-diCo and BcII-diZn are essentially identical. In addition, the overall higher resolution of our atomic models allowed us to disclose crucial aspects of BcII structure, which stem from an eased conformational plasticity of active-site loops, leading to adaptable metal coordination geometries.

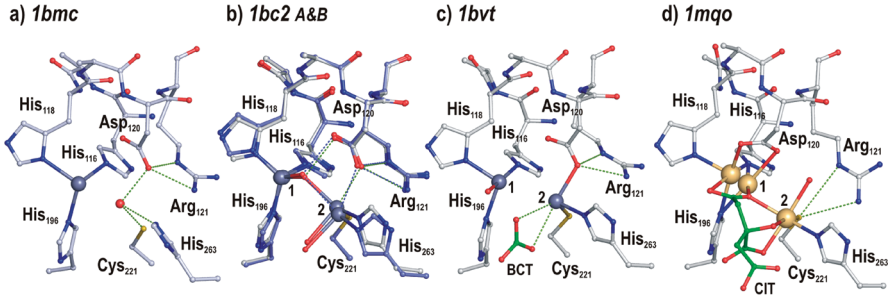

FIGURE 2: Metal-binding sites of available wild-type BcII crystal structures. PDB entries for Zn(II)-BcII: (a) 1bmc (*9*), (b) 1bc2 (*20*) (chains A and B overlaid, chain B colored dark blue), (c) 1bvt (*42*) (with a bicarbonate anion bound, BCT), and (d) 1mqo [corresponding to the Cd(II)-substituted form, with a double conformation for Cd(II) in the 3H site and a citrate anion bound, CIT]. Main chains of residues His196, Cys221, and His263 have been omitted for the sake of clarity. Dotted lines indicate selected noncovalent interactions, with distances in the range of 2.5−3.6 Å. Indicated metal coordination bond distances are in the range of 2.2−2.7 Å.

MATERIALS AND METHODS

Chemicals and Protein Samples. Analytical grade chemical reagents were commercially available. Sodium cacodylate, $ZnSO_4$, $CoSO_4$, and Chelex 100 resin were purchased from Sigma. Polyethylene glycol (PEG) 3350 was purchased from Hampton Research. Recombinant Zn(II)-BcII protein was expressed and purified as described previously (*18*). diCo(II)-BcII was prepared by titration of the apoprotein with $CoSO_4$, as reported by us (*25*). Protein concentrations were determined spectrophotometrically, using a molar extinction coefficient ε_{280} of 30500 M^{-1} cm^{-1} (*41*).

Crystallogenesis, Data Collection, and Phasing. Crystals of Zn(II)- and Co(II)-BcII were obtained by the hanging-drop vapor-diffusion method, using 24-well plates (Hampton Research), with 2 μL drops (1:1 protein:reservoir) and 1 mL reservoir solutions [100 mM sodium tartrate, 18% (w/v) PEG 3350, and 100 mM sodium cacodylate (pH 5.8); adapted from Carfi et al. (*42*)]. Protein was used at 200−250 μM, in 10 mM Tris-HCl (pH 7) and 50 mM NaCl. When necessary, an additive such as 1 mM DTT, $ZnSO_4$, or $CoSO_4$ was also added. Diffraction quality crystals appeared within 3−5 days of incubation at 20 °C.

The first attempts to obtain Co(II)-BcII crystals followed a crystallization approach analogous to that reported for Zn(II)-BcII (*42*), with zinc being replaced with cobalt. However, oxidation of residue Cys221 to Cys-sulfonate (Ocs) in the cobalt surrogate could not be avoided, even by using high $CoSO_4$ concentrations (up to 100 mM) or via addition of other reducing agents such as 2 mM TCEP or sodium ascorbate. Eventually, Co(II)-BcII crystals were obtained by exchanging Zn(II) for Co(II), directly in the crystals. To this end, Zn(II)-BcII crystals were harvested and soaked for 15 min in 10 μL drops of metal-free ML, containing 100 mM sodium tartrate, 18% (w/v) PEG 3350, 100 mM sodium cacodylate (pH 5.0), and 1 mM DTT. The ML was pretreated with Chelex 100 resin to remove trace divalent cations. This soaking procedure was repeated three times, always in metal-free drops. The resulting crystals were employed to collect X-ray diffraction data, which gave rise to atomic models for the apoprotein, thus validating the methodology for metal extraction. We then used apoprotein crystals to produce diCo(II)-BcII crystals by soaking them for 10 min in ML at pH 5.8, supplemented with 1 mM $CoSO_4$. Prior to data collection, crystals were mounted in a nylon loop and cryoprotected with ML supplemented with 20% (v/v) glycerol and flash-frozen in the liquid nitrogen stream (100 K).

Diffraction data were collected in house (Unit of Protein Crystallography, Institut Pasteur de Montevideo, Montevideo, Uruguay), with a MicroMax-007HF X-ray source (Rigaku) and a MAR345 image plate detector (Mar Research). Data processing was performed with MOSFLM (*43*) and SCALA (*44*) within the CCP4 suite of programs (*45*). Reflection intensities were included to the maximum resolution achievable for an average $I/\sigma(I)$ of 2.0. Molecular replacement was performed using AMORE (*46*) with PDB entry 1bvt as a search probe. To minimize model bias prior to refinement procedures, the MR solution model was subjected to a random shift of 0.2 Å in all the atomic coordinates and a constant *B* factor corresponding to the Wilson plot slope was assigned to all atoms.

Refinement of Atomic Models. Maximum-likelihood restrained refinement was performed with REFMAC5 (*47*). Reciprocal space refinement rounds were iterated with manual model rebuilding using σ_A-weighted $2F_O - F_C$ electron density maps. Once most of the protein backbone and amino acid side chains had been built, the metal ions and structured water molecules were readily discernible as strong positive peaks in difference Fourier $F_O - F_C$ maps. During the refinement of metal ion positions, no distance restraints were applied for coordination bonds. Occupancies in DCH-site metal ions were manually adjusted, seeking to reach the best agreement among refined *B* factors of interacting atoms.

Model building was performed with COOT (*48*). Model validation was done throughout the refinement with the built-in functions of COOT. PROCHECK (*49*) and SFCHECK (*50*) were used for validation of the final models. Graphic representations of molecular structures were prepared with PYMOL v0.99rc6 (*51*).

For BcII-diCo and BcII-Gol structures, the metal identity was corroborated by inspection of $F_{(+)} - F_{(-)}$ anomalous difference maps, given the significant anomalous signal of Co at 1.5418 Å.

The glycerol ligand in the active site of BcII-Gol was modeled with the aid of an isomorphous $F_{Gol} - F_{Ocs}$ difference map, whose coefficients are the differences between scaled reflection intensities of partially and fully oxidized BcII, respectively. The corresponding amplitudes for BcII-Gol (F_{Gol}) and BcII-Ocs (F_{Ocs}) were scaled with SCALEIT (*45*).

In the last stages of refinement, anisotropic *B* factor refinement was applied for selected atoms (namely, Co1 atom in BcII-Ocs; all atoms in BcII-diCo; and Co1, Co2, and the imidazole group of the His118 side chain in BcII-Gol). This procedure significantly improved the R_{free} in subsequent refinement cycles, validating its pertinence.

RESULTS

Cysteine 221 Is Highly Sensitive to Oxidation in Co(II)-BcII. The first crystallization trials of Co(II)-substituted BcII gave rise to a monometallic variant, with residue Cys221 oxidized to Cys-sulfonate (residue Ocs221), BcII-Ocs, which was refined to 1.55 Å resolution (Tables 1 and 2). BcII-Ocs shows a single Co(II) ion in the 3H site (Co1), with the Ocs221 sulfonate group coordinated to Co1, 2.5 Å apart (Figure 3a). As a result, the Co(II) ion exhibits a distorted octahedral geometry with His116, His118, His196, Ocs221, and two water molecules (w_B and w_D) occupying the six coordination positions. Oxidation of Cys221 induces a conformational change at the C-terminus of loop L7 (spanning residues His116−Arg121), particularly residues Ala119 and Asp120, which exhibit two alternate positions.

Freshly prepared Co(II)-BcII crystals allowed us to refine a structure of di-Co(II) BcII at 1.55 Å, where residue Cys221 is seen only partially oxidized [BcII-Gol (Tables 1 and 2)]. Given that electron density in the metal binding site is averaged between the reduced and oxidized populations of BcII (i.e., BcII-diCo and BcII-Ocs), its interpretation required the inspection of several maps, namely, electron density $2F_O - F_C$, Fourier difference $F_O - F_C$, anomalous difference $F_{(+)} - F_{(-)}$, and isomorphous difference between observed reflections of BcII-Gol and BcII-Ocs, $F_{Gol} - F_{Ocs}$. It is worth emphasizing that a significant anomalous signal from cobalt absorption (K-edge at 1.6085 Å) is available at the copper anode emission wavelength (1.5418 Å).

Although the $2F_O - F_C$ electron density map at residue Cys221 suggests some degree of oxidation (Figure 4a), the $F_{(+)} - F_{(-)}$ anomalous difference map indicated the presence of Co(II) in the DCH site (Figure 4b), thus revealing the presence of reduced Cys221 as well. Partially occupied Ocs221 prompted us to search also for alternate conformations for loop L7 and water molecule

Table 1: Diffraction Data Collection Statistics

	BcII-Ocs	BcII-Apo	BcII-diZn	BcII-diCo	BcII-Gol
space group	*C*2	*C*2	*C*2	*C*2	*C*2
cell constants					
a (Å)	53.2	53.0	53.1	53.1	53.1
b (Å)	61.8	61.6	61.4	61.4	61.7
c (Å)	69.5	69.5	69.5	65.6	69.6
β (deg)	93.2	93.0	93.1	93.0	93.1
no. of unique reflections	30132	27504	21061	35794	31080
B factor (Wilson) (Å^2)	22.4	23.8	24.6	23.0	24.5
solvent content (%)	43.1	46.5	47.3	43.4	42.5
resolution range (Å)					
overall	40.3−1.55	17.1−1.60	20.5−1.74	40.1−1.45	40.2−1.55
outer shell	1.6−1.55	1.69−1.60	1.83−1.74	1.53−1.45	1.63−1.55
R_{merge} [a]	0.049 (0.363)	0.037 (0.364)	0.024 (0.401)	0.057 (0.374)	0.028 (0.156)
completeness (%) [a]	91.3 (77.8)	93.3 (91.3)	92.0 (90.1)	90.5 (84.0)	95.4 (87.2)
$\langle I/\sigma(I)\rangle$ [a]	18.4 (3.1)	15.6 (2.2)	12.5 (2.0)	15.5 (2.0)	34.1 (9.9)
multiplicity	3.6	2.2	2.1	3.5	6.0

[a] Outer-shell values are in parentheses.

Table 2: Structure Refinement Statistics

	BcII-Ocs	BcII-Apo	BcII-diZn	BcII-diCo	BcII-Gol
PDB entry	3i15	3i0v	3i13	3i11	3i14
resolution range (Å)	40.3−1.55	17.1−1.60	20.5−1.74	40.1−1.45	35.4−1.55
R_{cryst} (all reflections) (%)	15.1	16.1	15.9	16.2	15.7
R_{free} (5% free set) (%)	18.6	20.5	21.7	20.4	19.1
no. of atoms					
protein	1710	1671	1658	1713	1741
metal ion	1	0	2	2	2
solvent	266	226	220	238	254
ligand	−	−	−	−	6
average *B* factor (Å^2)					
protein	18.1	24.3	24.0	27.0	16.1
3H site					
first coordination shell	19.3	−	20.9	22.7	18.4
metal 1	24.2	−	30.9	23.1	25.6
DCH site					
first coordination shell	−	−	29.3	30.5	23.9
metal 2	−	−	37.4	28.2	25.1
deviations from ideality					
rmsd for bonds (Å)	0.020	0.022	0.021	0.021	0.021
rmsd for angles (deg)	1.784	1.852	1.760	1.782	1.950
Murshudov's DPI (Å)	0.076	0.088	0.12	0.071	0.077
Ramachandran outliers	4 (2.02%)	3 (1.52%)	2 (0.99%)	3 (1.52%)	2 (1.06%)

w_D found in BcII-Ocs (Figure 3a). Once this region was modeled with half-occupancy for the BcII-diCo and BcII-Ocs contributions, a noteworthy improvement of the difference Fourier $F_O - F_C$ map was achieved, particularly in the loop L7 backbone region. These refinement steps were critically aided by inspection of the $F_{Gol} - F_{Ocs}$ isomorphous difference map (Figure 4c), which clearly showed that the reduced fraction of BcII-Gol exhibits an octahedral center at Co2, w_B bridging water/OH^- molecule, and a solvent ligand (positive density), as well as the absence of Ocs221 and w_D (negative density). Finally, the ligand bound in the active site could be modeled as a glycerol molecule, H-bonded to the backbone N atom of Asn233 (2.7 Å from GolO1), and coordinated to Co2 2.3 Å from GolO2 and GolO3.

Removal of Zn(II) from BcII Crystals. Aiming to circumvent the problem of Co(II)-promoted Cys221 oxidation, we explored different strategies for minimizing the exposure of BcII to Co(II). Because BcII is inactivated at acidic pH by metal dissociation in solution (*24*), we attempted metal removal in crystals by decreasing the pH. Effectively, BcII crystals withstand metal depletion through soaking in a mother liquor adjusted at pH 5, without a loss of diffraction quality. We assessed the absence of Zn(II) ions in the metal-depleted crystals by collecting diffraction data sets and determining the corresponding structure, BcII-Apo, refined at 1.60 Å (Tables 1 and 2). In this case, the intense $F_O - F_C$ positive density peaks typically found at Zn1 and Zn2 sites of the metalated forms were undetectable. Moreover, the conformations of amino acid side chains that participate in the metal binding sites were significantly changed, as judged by comparison with wild-type BcII. The most remarkable feature was observed for His116 and His118 side chains, both showing two alternate conformations (A and B), all of them moved away from the wild-type positions (Figure 3b). A water molecule is found near the position occupied by Zn1, located 3.2, 2.7, and 2.8 Å from His116B Nδ1, His118A Nδ1, and His196 Nε2, respectively. Such rather long distances allow us to discard a low-occupancy Zn(II) ion in this site, normally 2.0−2.2 Å from

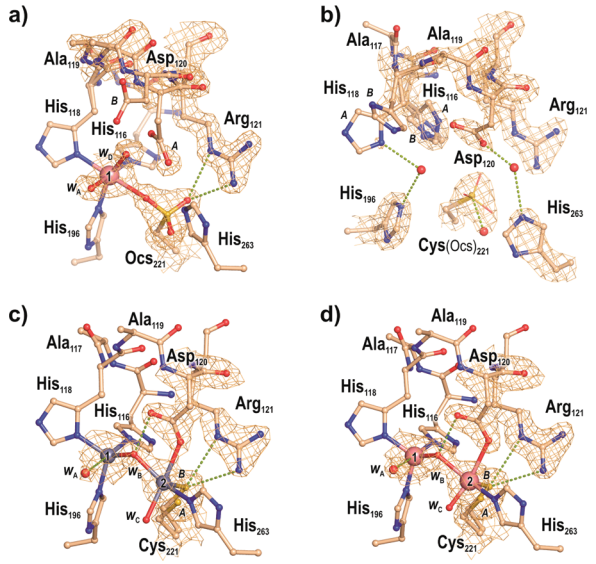

FIGURE 3: Structure of the active site determined for (a) BcII-Ocs, (b) BcII-Apo, (c) BcII-diZn, and (d) BcII-diCo. Electron density in selected regions is depicted as a wireframe surface, contoured at 1σ (BcII-Ocs, BcII-diZn, and BcII-diCo) or 1.5σ (BcII-Apo). Density for some His side chains has been omitted for the sake of clarity. Electron density in loop HAHADR of BcII-diZn and BcII-diCo is shown for residue Asp120 and Arg121 side chains only (see the text for details). Numbers 1 and 2 indicate metal ions in the 3H and DCH sites, respectively. Selected noncovalent interactions are represented as green dotted lines.

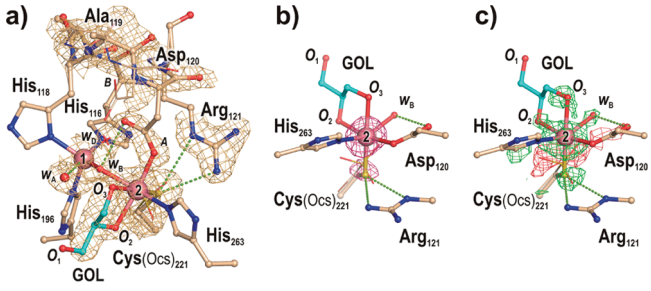

FIGURE 4: Active site of partially oxidized di-Co(II) BcII, BcII-Gol. (a) Electron density in selected regions is depicted as a wireframe surface, contoured at 1σ (with His side chain density omitted for the sake of clarity). Alternate conformations of loop HAHADR, Ocs221, and water molecule w_D found in BcII-Ocs are shown as thin lines (compare with Figure 1a). (b) Anomalous difference $F_{(+)} - F_{(-)}$ map (pink wireframe, 5σ), highlighting the presence of Co(II) in the DCH site. (c) Isomorphous difference $F_{Gol} - F_{Ocs}$ map in the DCH site, emphasizing the octahedral geometry of Co2 (3.5σ, green wireframe), as well as the absence of Ocs221 in the reduced fraction of BcII-Gol (−3.5σ, red wireframe). Numbers 1 and 2 indicate Co(II) ions in the 3H and DCH sites, respectively. Selected noncovalent interactions are represented as green dotted lines.

His imidazole N atoms. A comparable situation is witnessed for the DCH site, where the His263 side chain appears to be flipped around the Cβ−Cγ axis, H-bonded to the side chain of Asp120 through a solvent molecule. Altogether, these features clearly evince the absence of metals in the 3H site, confirming the success of our crystal metal depletion approach. The electron density distribution in Cys221 Sγ was suggestive of some degree of oxidation, possibly due to circumstantial air exposure of the apoprotein crystals during handling, which was modeled as 80% reduced Cys. It is noteworthy that loop L7 in BcII-Apo exhibits a single conformation with a well-defined electron density, in contrast with the structure of BcII-Ocs (where Cys221 is fully oxidized).

The Structure of BcII-Co(II) Is Equivalent to That of Wild-Type BcII. We prepared Co(II)-BcII crystals by soaking apoprotein crystals in a Co(II)-based mother liquor. Diffraction data sets of these crystals allowed us to obtain a high-resolution structure of Co(II)-substituted BcII. In addition, we determined the structure of Zn(II)-BcII under the same conditions so that reliable comparisons with the Co(II) surrogate could be made. The structures of diZn(II)-BcII (BcII-diZn hereafter) and diCo-(II)-BcII (BcII-diCo hereafter) were refined at 1.74 and 1.45 Å, respectively (see Tables 1 and 2). Both atomic models are identical within experimental error, with a root-mean-square deviation of 0.10 Å for superimposition of 214 residues (1489 atoms). With regard to the metal binding sites, both Zn(II) and Co(II) ions display comparable coordination environments (Figure 3c,d), with a half-occupied DCH site.

The 3H site exhibits a coordination number of four in both adducts, with the metal ions bound to His116, His118, His196, and the bridging water/OH^- molecule, w_B, 2.0 and 2.1 Å from Co1 and Zn1, respectively. An additional water molecule, w_A, is located within electrostatic interaction distance of Co1 and Zn1, at 2.8 Å. Thus, the 3H-site geometry can be described as tetrahedral with a trigonal-bipyramidal distortion along the w_A−Zn1/Co1−His116 Nε2 axis. Contrasting the situation witnessed for BcII-Ocs and BcII-Apo, loop HAHADR adopts a conformation that positions the Asp120 side chain coordinated to Co2 and Zn2 (at 2.5 and 2.4 Å, respectively) and H-bonded to water/OH^- molecule w_B (2.5 Å for both BcII-diCo and BcII-diZn). The Co1−Co2 and Zn1−Zn2 distances are equivalent (ca. 3.7 Å), considering the estimated coordinate errors (Table 2).

The metal ions at the DCH site are both five-coordinate, being bound to Asp120, Cys221, His263, and two water molecules, w_A and w_B (Figure 3c,d). The geometry can be described as distorted trigonal-bipyramidal, with an Asp120 Oδ2−Zn2/Co2−w_C principal axis, Cys221, His263, and w_B lying in the equatorial plane. While 3H sites of BcII-diCo, BcII-diZn, and BcII-Gol (reduced fraction) are similar, the equivalent position of Gol O2 in BcII-Gol is occupied by water molecule w_C in BcII-diCo and BcII-diZn (1.9 and 2.2 Å from Co2 and Zn2, respectively), and that of Gol O3 remains vacant (compare panels c and d of Figure 3 with Figure 4a).

While residues Asp120 and His263 display well-defined conformations, residue Cys221 exhibits two half-occupied alternate positions, A and B. The Sγ−Co2 and Sγ−Zn2 distances are 1.8 Å for conformer Cys221A and 2.3 Å for conformer Cys221B. Given that Cys221A Sγ is too close to Co2 or Zn2, only conformer Cys221B can be regarded as a metal ligand for each DCH-site metal ion. This assumption is in good agreement with the metal site half-occupancy and the expected metal−thiolate bond distances for Co(II) and Zn(II). Besides, conformer B of Cys221 is reminiscent of the Cys221 position found in the reduced fraction of BcII-Gol, where Cys221 Sγ is 2.3 Å from Co2.

The double conformation of residue Cys221 entailed a largely anisotropic electron density distribution at Sγ. Because BcII harbors two contiguous Gly residues adjacent to Cys221, Gly219, and Gly220, suggesting that this portion in loop L10 is flexible, we determined that the model could be improved by refining Gly220 also in two half-occupied conformations, thereby providing additional conformational freedom to residue Cys221. As a result, a separation of ca. 0.3, 0.5, and 1.0 Å was achieved during refinement between corresponding Cα, Cβ, and Sγ atoms of Cys221 alternate positions. On the other hand, conformer

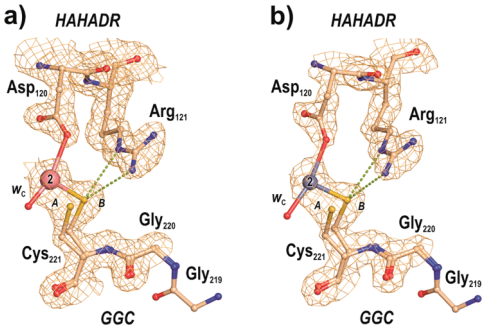

FIGURE 5: Electrostatic interaction (green dotted lines) between Arg121 and Cys221 side chains in (a) BcII-diCo and (b) BcII-diZn. An electron density $2F_O - F_C$ map (at 1σ) is shown as a wireframe surface for metal ions and residues Asp120 and Arg121 (in loop HAHADR) and residues Gly220 and Cys221 (in loop GGC).

Cys221B is found within salt bridging distance of the Arg121 side chain, with Sγ located ~3.2 Å from the guanidinium moiety. Therefore, the flexibility of the Gly219−Cys221 stretch is expected to significantly restrain the position of the DCH-site metal ion through both first-shell and second-shell effects, i.e., by influencing the corresponding interactions with Cys221 and Arg121 (Figure 5).

DISCUSSION

Flexibility of Loop L7. One of the most outstanding structural features of metallo-β-lactamases is that the metal binding sites are entirely built on loops and turns (*9*, *15*, *20*, *21*, *23*, *52*, *53*). The presence of two protruding loops (L3 and L10) that flank the active site has been interpreted as a requirement for binding and hydrolyzing a large variety of β-lactam antibiotics. Via analysis of the five structures reported here, two additional regions emerge as conformationally adaptable: loops L7 and the GGC stretch in the base of loop L10 (Figure 1) (*54*). L7 (His116−Arg121) contains three metal ligands (His116 and His118, involved in the 3H site; and Asp120, a ligand at the DCH site), whereas the GGC region (Gly219−Cys221) contains residue Cys221, a DCH-site ligand. Because these two regions harbor four of the six metal-liganding residues in the protein, their conformations are not independent of one another, evidently restraining both metal coordination environments.

Structures BcII-Ocs, BcII-Gol, and BcII-Apo provide insights into the flexibility of loop L7. The structure of BcII-Ocs displays a single 3H-site Co(II) ion with residue Cys221 oxidized to Cys-sulfonate (Ocs221) (Figure 3a), and the same scenario can be witnessed for the oxidized fraction of BcII-Gol (Figure 4a). Loop L7 can accommodate the presence of a negatively charged sulfonate group by adjusting the conformation of residues Ala119 and Asp120, with minimal changes in the conformation of His116, His118, and Arg121 side chains, as compared with the wild-type conformations (Figure 3c,d). On the other hand, the structure of BcII-Apo displays double conformations for His116 and His118 side chains, while Asp120 and Arg121 remain nearly unaffected (Figure 3b), revealing a key role for Zn1 in shaping the 3H site. Notwithstanding, the architecture of loops flanking the active-site cavity is largely preserved in BcII-Apo, corroborating the report that the apoenzyme's inability to bind any substrate is mainly due to the absence of the metal ions (*55*).

Flexibility of the GGC Stretch. The loop L10 segment comprising residues Gly219, Gly220, and Cys221 (GGC) also

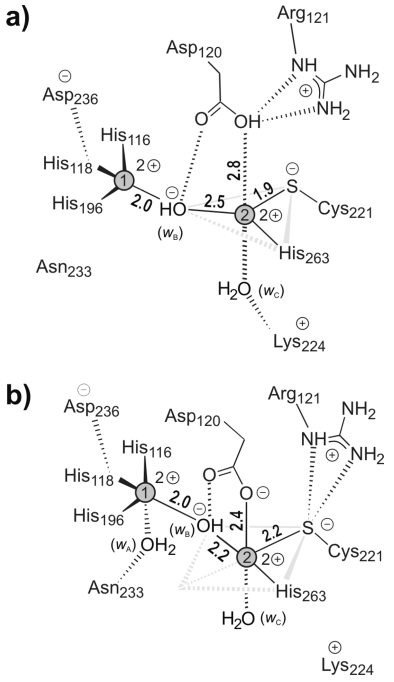

FIGURE 6: Schematic representation of the metal coordination environments in wild-type BcII structures of PDB entries (a) 1bc2 and (b) 3i13 (depicting conformer Cys221B only, as obtained in this work), illustrating the structural rearrangements leading to changes in the coordination number of Zn2. Dashed black lines indicate noncovalent interactions. Gray lines depict an equatorial plane defined for Zn2. Numbers indicate selected distances (in angstroms) and the metal ions (gray circles).

exhibited a remarkable conformational freedom, most likely due to the presence of two contiguous Gly residues, allowing alternate conformations for residue Cys221. Previous studies suggest that residue Cys221 critically influences the DCH-site metal binding affinity. Cys221Ser mutants (*56*), as well as the double mutant Cys221Ser/Arg121His (*57*), display a sequential metal binding mode, i.e., a Zn2 site with significantly lower affinity than the Zn1 site. Besides, several Asp120 mutants of BcII retain their Zn2 binding capability, although the β-lactamase activity spectrum is severely compromised (*58*). Consequently, given that Gly219 and Gly220 are conserved among B1 MβLs (*59*), these residues were probably selected to grant the conformational adaptability of the Cys221 side chain, ultimately influencing the position of Zn2 and catalysis.

The GGC region flexibility also endows an ionic interaction between Cys221 thiolate and Arg121 guanidinium groups, located in the second coordination shell of Zn2. Such interaction would be relevant when residue Asp120 is deprotonated, preferentially coordinated to Zn2 (Figure 6). Earlier structures of Zn(II)-BcII show that the Asp120 side chain interacts electrostatically with the Arg121 side chain (*19*, *42*), and similar scenarios have been described for other B1 MβLs sharing an Arg121 residue, such as VIM-2 (*52*) and BlaB (*60*). Residue Arg121 is thus believed to keep the Asp120 carboxylate deprotonated, thereby increasing the metal affinity and broadening the optimal pH range of the enzyme (*12*, *58*). Our observations disclose an additional mode for Arg121 to influence the DCH-site metal ion, that is, by interacting with Cys221 thiolate. As a result, Arg121, Asp120, Cys221, and Zn2 comprise an arrangement of two pairs of opposite charge ions in equilibrium. In this way, the Arg121 residue would also enhance the Zn2 electrophilicity by interacting with the negatively charged Asp120 and Cys221

ligands (Figure 6). This suggestion is particularly attractive, considering that a fundamental role of Zn2 in the catalytic pathway is the stabilization of anionic intermediates of β-lactams.

Two MβL subclasses share a Cys221 residue, namely, the broad-spectrum enzymes from the B1 group and the exclusive carbapenemases from group B2. B1 enzymes bear the conserved GGC stretch that, as we now show, appears to play a key role in facilitating the Arg121−Cys221 interaction, ultimately regulating the conformational freedom of Cys221. Instead, B2 enzymes share the GNC sequence (Gly219, Asn220, and Cys221), along with the conserved residue Asn116 (replacing the conserved His116 in B1 enzymes) (*59*). The B2 enzyme CphA from *Aeromonas hydrophila* has been crystallized in complex with carbonate (PDB entry 1x8g), captopril (PDB entry 2qds), a pyridinecarboxylate (PDB entry 2gkl), and even di-Zn(II) (PDB entry 3f9o). Despite the variety of bound ligands, the active-site backbone region is minimally altered, strongly suggesting an intrinsic rigidity of loops L7, L9, and L12 in B2 lactamases. Furthermore, two H-bonds are retained between residues Asn116 and Asn220. The double mutant Asn116His/Asn220Gly of CphA has been shown to exhibit a significantly broader substrate spectrum than wild-type CphA (*61*), whereas the mutant Asn220Gly exhibits considerably lower k_{cat} and K_M values against biapenem, leading to product inhibition and the consequent feasibility of a crystallographic structure for this complex (PDB entry 1x8i) (*21*). Altogether, the lower flexibility exhibited by B2 enzymes in this region explains their higher substrate specificity. We hence propose that the GGC loop conformational flexibility critically contributes to substrate promiscuity, a trait characteristic of B1 enzymes.

Previous studies show that mutations restraining the conformation of Cys221 lead to changes in the catalytic spectrum. Mutant Gly262Ser of BcII exhibits higher activity against cephalexin and nitrocefin, and lower activity against imipenem, as compared to wild-type BcII (*54*). As determined by X-ray crystallography (PDB entry 3fcz), mutant Gly262Ser BcII displays an H-bond between Ser262 and Cys221 side chains. This arrangement favors a position of Zn2 more accessible to the active-site groove (*54*), with Cys221 resembling conformer Cys221A. Comparable changes in the activity profile have been observed for IMP-1 β-lactamase, a natural Gly262Ser mutant of the IMP-6 enzyme, where the IMP-1 enzyme exhibits increased activity against ceftazidime, benzylpenicillin, ampicillin, and imipenem, versus the activities of the IMP-6 enzyme (*62*).

Finally, it is worth noting that crystallographic structures of Arg121-containing B1 MβLs typically display a Zn2 ion with partial occupancy. This feature was attributed to residue Arg121, which provides a positive charge in the vicinity of Zn2. However, this hypothesis was ruled out in light of mutagenesis studies of residues Arg121 and Asp120, because the mutant Arg121Cys structure also exhibits fractional occupancy for Zn2 (*63*), and several Asp120 mutants display Zn(II) affinities at the DCH site comparable to that of wild-type BcII (*58*). The alternate conformations of Cys221, granted by the conformational flexibility of the GGC stretch, provide a simple explanation for the fractional occupancy of Zn2 in these structures.

Structural Consequences of Metal Substitution in BcII. Cobalt substitution has been regarded as one the most conservative strategies for spectroscopic studies in zinc enzymes. This is due to the fact that, despite their different electronic structures, the native activity is generally preserved upon Co(II) uptake. The ligand-field bands of the Co(II)-BcII electronic spectrum comprise a four-band pattern characteristic of distorted tetrahedral three-His Zn(II) sites, like those found in Co(II)-substituted carbonic anhydrase II (*64*) and the insulin hexamer (*65*). The BcII-diCo and BcII-Gol structures clearly show that Co(II) adopts a distorted tetrahedral geometry in the 3H site, with an identical coordination sphere compared with that of BcII-diZn, thus supporting the assignment of these spectral features to the 3H-site Co(II). Taking into account the coordination number of five or six for the DCH-site Co(II) ion (as shown for the BcII-diCo or BcII-Gol structure, respectively), we conclude that its contribution to the ligand-field bands would be minimal. Therefore, the structures of Co(II)-substituted BcII disclosed here provide evidence accounting for the lower molar extinction of the DCH-site Co(II) ligand-field bands (*30*), as previously suggested (*18*).

It has been stressed that some organic complexes of Co(II) tend to expand the coordination sphere compared with Zn(II) (*66*), and additional solvent molecules have been found in protein Zn(II) sites substituted with Co(II) (*67*). We can confirm that this is not the case for BcII, where both Zn(II) and Co(II) surrogates exhibit nearly identical coordination environments (Figure 3c,d). In addition, we found that the DCH site can accommodate a bound glycerol molecule in the presence of Co(II), which has not been reported for the Zn(II) substitute so far. Via comparison of the DCH sites of BcII-diCo and BcII-Gol, minimal changes in the coordination angles are observed, indicating that glycerol binding occurs without affecting the metal ion coordination geometry. As a result, the DCH-site five-coordinate metal shell can be regarded as a distorted octahedral geometry with one vacant coordination position, which is available to interact with the substrate (compare Figures 3d, 4, and 6). Hence, our structures do not evince a general expansion of the Co(II) coordination sphere but reflect an enhanced binding ability of Co(II) over Zn(II) under certain conditions, most probably related to the inherent chemical properties of each metal ion. This observation concurs with the β-lactamase catalytic efficiencies reported for each surrogate, which can differ substantially depending on the antibiotic (*29*, *36*, *68*).

The BcII-Gol structure shows that the metal in the DCH site can interact with a bidentate ligand (Figure 4), a binding mode previously determined by X-ray crystallography for Cd(II)-BcII with citrate and L1 β-lactamase from *Stenotrophomonas maltophilia* with hydrolyzed moxalactam (*23*). These complexes suggest that the intact antibiotics would also bind as bidentate ligands, enabling a proper interaction of Zn2 with the β-lactam ring N atom. Such a role for Zn2 has been established for several anionic intermediates, like those of biapenem and moxalactam in CphA and L1, respectively (*21*, *23*), as well as imipenem and meropenem in BcII (*4*), and nitrocefin in CcrA, L1, and GOB-18 (*26*, *69*). In the case of BcII against benzylpenicillin, no anionic intermediates have been detected, although some reaction intermediates have been proposed to imply a hexacoordinate DCH-site metal ion (*3*). The d^{10} configuration of Zn(II) favors changes in its coordination geometry with minimal energy costs. Nonetheless, considering the diversity of substrates sensitive to B1 MβL-mediated hydrolysis, the first and second metal coordination shells provided by the protein environment must allow for these geometry changes. In fact, BcII can also accommodate dissimilar metal ions like Cd(II) and Mn(II). A high-resolution (1.35 Å) structure of Cd(II)-substituted BcII (PDB entry 1mqo) is available, with a citrate anion (CIT) bound to the active site (Figure 2d). In this structure, Cd2 is hexacoordinated to the DCH site and three functional groups of the CIT ligand. Despite the

longer ionic radius of Cd(II) (1.09 Å) compared to those of Zn(II) and Co(II) (0.88 and 0.84 Å, respectively) (*70*), together with its acknowledged preference for higher coordination numbers, Cd(II)-substituted BcII is an active β-lactamase (*29*). Similar results have been reported for the Mn(II)-substituted enzyme, where β-lactamase activity is preserved despite the Mn(II) predilection for octahedral coordination geometries (*70*). This adaptability of BcII toward metal substitution is in sharp contrast with that of enzymes like thermolysin and human carbonic anhydrase II, which are active as Zn(II) and Co(II) surrogates but are inhibited by Cd(II) (*71*, *72*). Furthermore, Breece and co-workers have recently disclosed the presence of changes in the Zn−Zn distance during turnover of the B3 enzyme L1 (*73*). Despite the fact that there is no experimental evidence of these changes in B1 enzymes, molecular dynamics simulations (*14*, *74*) and QMMM calculations support this notion. In this context, the flexibility of regions HAHADR (in L7) and GGC (in L10) that we report assists in taking full advantage of the Zn(II) coordination adaptability, minimizing the activation energy for hydrolysis.

CONCLUDING REMARKS

In this work, the active site of *B. cereus* Zn(II)-dependent metallo-β-lactamase is interrogated through X-ray crystallography, by analysis of the structural effects taking place upon Co(II) substitution, changes in metal content, and crystallization conditions. The high degree of similarity of the active-site structure of the Co(II) and Zn(II) adducts strongly supports the use of Co(II) substitution in these enzymes. While a general good agreement is observed with previously determined structures for the Zn(II) derivative, the structures reported here show that the loops containing key metal ligand residues display a remarkable conformational flexibility. In light of the proposed catalytic mechanisms for this enzyme, such adaptable coordination environments would enable interaction with different substrates, thus favoring promiscuity rather than proficiency toward specific substrates.

REFERENCES

1. Fisher, J. F., Meroueh, S. O., and Mobashery, S. (2005) Bacterial resistance to β-lactam antibiotics: Compelling opportunism, compelling opportunity. *Chem. Rev. 105*, 395–424.
2. Crowder, M. W., Spencer, J., and Vila, A. J. (2006) Metallo-β-lactamases: Novel Weaponry for Antibiotic Resistance in Bacteria. *Acc. Chem. Res. 39*, 721–728.
3. Llarrull, L. I., Tioni, M. F., and Vila, A. J. (2008) Metal Content and Localization during Turnover in *B. cereus* Metallo-β-lactamase. *J. Am. Chem. Soc. 130*, 15842–15851.
4. Tioni, M. F., Llarrull, L. I., Poeylaut-Palena, A. A., Martí, M. A., Saggu, M., Periyannan, G., Mata, E. G., Bennett, B., Murgida, D. H., and Vila, A. J. (2008) Trapping and Characterization of a Reaction Intermediate in Carbapenem Hydrolysis by *B. cereus* Metallo-β-lactamase. *J. Am. Chem. Soc. 130*, 15852–15863.
5. Spencer, J., and Walsh, T. R. (2006) A new approach to the inhibition of metallo-β-lactamases. *Angew. Chem., Int. Ed. 45*, 1022–1026.
6. Drawz, S. M., and Bonomo, R. A. (2010) Three decades of β-lactamase inhibitors. *Clin. Microbiol. Rev. 23*, 160–201.
7. Galleni, M., Lamotte-Brasseur, J., Rossolini, G. M., Spencer, J., Dideberg, O., and Frere, J. M. (2001) Standard numbering scheme for class B β-lactamases. *Antimicrob. Agents Chemother. 45*, 660–663.
8. Bebrone, C. (2007) Metallo-β-lactamases (classification, activity, genetic organization, structure, zinc coordination) and their superfamily. *Biochem. Pharmacol. 74*, 1686–1701.
9. Carfi, A., Pares, S., Duee, E., Galleni, M., Duez, C., Frère, J. M., and Dideberg, O. (1995) The 3-D structure of a zinc metallo-β-lactamase from *Bacillus cereus* reveals a new type of protein fold. *EMBO J. 14*, 4914–4921.
10. Daiyasu, H., Osaka, K., Ishino, Y., and Toh, H. (2001) Expansion of the zinc metallo-hydrolase family of the β-lactamase fold. *FEBS Lett. 503*, 1–6.
11. Dal Peraro, M., Vila, A. J., and Carloni, P. (2002) Structural determinants and hydrogen-bond network of the mononuclear zinc(II)-β-lactamase active site. *J. Biol. Inorg. Chem. 7*, 704–712.
12. Dal Peraro, M., Vila, A. J., and Carloni, P. (2003) Protonation state of Asp120 in the binuclear active site of the metallo-β-lactamase from *Bacteroides fragilis*. *Inorg. Chem. 42*, 4245–4247.
13. Dal Peraro, M., Vila, A. J., and Carloni, P. (2004) Substrate binding to mononuclear metallo-β-lactamase from *Bacillus cereus*. *Proteins 54*, 412–423.
14. Dal Peraro, M., Vila, A. J., Carloni, P., and Klein, M. L. (2007) Role of zinc content on the catalytic efficiency of B1 metallo β-lactamases. *J. Am. Chem. Soc. 129*, 2808–2816.
15. Concha, N. O., Janson, C. A., Rowling, P., Pearson, S., Cheever, C. A., Clarke, B. P., Lewis, C., Galleni, M., Frere, J. M., Payne, D. J., Bateson, J. H., and Abdel-Meguid, S. S. (2000) Crystal structure of the IMP-1 metallo β-lactamase from *Pseudomonas aeruginosa* and its complex with a mercaptocarboxylate inhibitor: Binding determinants of a potent, broad-spectrum inhibitor. *Biochemistry 39*, 4288–4298.
16. Yamaguchi, Y., Jin, W., Matsunaga, K., Ikemizu, S., Yamagata, Y., Wachino, J., Shibata, N., Arakawa, Y., and Kurosaki, H. (2007) Crystallographic investigation of the inhibition mode of a VIM-2 metallo-β-lactamase from *Pseudomonas aeruginosa* by a mercaptocarboxylate inhibitor. *J. Med. Chem. 50*, 6647–6653.
17. Concha, N. O., Rasmussen, B. A., Bush, K., and Herzberg, O. (1996) Crystal structure of the wide-spectrum binuclear zinc β-lactamase from *Bacteroides fragilis*. *Structure 4*, 823–836.
18. Orellano, E. G., Girardini, J. E., Cricco, J. A., Ceccarelli, E. A., and Vila, A. J. (1998) Spectroscopic characterization of a binuclear metal site in *Bacillus cereus* β-lactamase II. *Biochemistry 37*, 10173–10180.
19. Fabiane, S. M., Sohi, M. K., Wan, T., Payne, D. J., Bateson, J. H., Mitchell, T., and Sutton, B. J. (1998) Crystal structure of the zinc-dependent β-lactamase from *Bacillus cereus* at 1.9 Å resolution: Binuclear active site with features of a mononuclear enzyme. *Biochemistry 37*, 12404–12411.
20. Carfi, A., Duee, E., Paul-Soto, R., Galleni, M., Frere, J. M., and Dideberg, O. (1998) X-ray structure of the ZnII β-lactamase from *Bacteroides fragilis* in an orthorhombic crystal form. *Acta Crystallogr. D54* (Part 1), 45–57.
21. Garau, G., Bebrone, C., Anne, C., Galleni, M., Frere, J. M., and Dideberg, O. (2005) A metallo-β-lactamase enzyme in action: Crystal structures of the monozinc carbapenemase CphA and its complex with biapenem. *J. Mol. Biol. 345*, 785–795.
22. Wang, Z., Fast, W., and Benkovic, S. J. (1999) On the mechanism of the metallo-β-lactamase from *Bacteroides fragilis*. *Biochemistry 38*, 10013–10023.
23. Spencer, J., Read, J., Sessions, R. B., Howell, S., Blackburn, G. M., and Gamblin, S. J. (2005) Antibiotic recognition by binuclear metallo-β-lactamases revealed by X-ray crystallography. *J. Am. Chem. Soc. 127*, 14439–14444.
24. Rasia, R. M., and Vila, A. J. (2002) Exploring the role and the binding affinity of a second zinc equivalent in *B. cereus* metallo-β-lactamase. *Biochemistry 41*, 1853–1860.
25. Llarrull, L. I., Tioni, M. F., Kowalski, J., Bennett, B., and Vila, A. J. (2007) Evidence for a dinuclear active site in the metallo-β-lactamase BcII with substoichiometric Co(II). A new model for metal uptake. *J. Biol. Chem. 282*, 30586–30595.
26. Lisa, M. N., Hemmingsen, L., and Vila, A. J. (2009) Catalytic role of the metal ion in the metallo-β-lactamase GOB. *J. Biol. Chem. 285*, 4570–4577.
27. de Seny, D., Heinz, U., Wommer, S., Kiefer, M., Meyer-Klaucke, W., Galleni, M., Frere, J. M., Bauer, R., and Adolph, H. W. (2001) Metal ion binding and coordination geometry for wild type and mutants of metallo-β-lactamase from *Bacillus cereus* 569/H/9 (BcII): A combined thermodynamic, kinetic, and spectroscopic approach. *J. Biol. Chem. 276*, 45065–45078.
28. Davies, R. B., and Abraham, E. P. (1974) Metal Cofactor Requirements of β-Lactamase II. *Biochem. J. 143*, 129–135.
29. Badarau, A., and Page, M. I. (2006) The Variation of Catalytic Efficiency of *Bacillus cereus* Metallo-β-lactamase with Different Active Site Metal Ions. *Biochemistry 45*, 10654–10666.
30. Bertini, I., and Luchinat, C. (1983) Cobalt(II) as a probe of the structure and function of carbonic anhydrase. *Acc. Chem. Res. 16*, 272–279.
31. Bicknell, R., Schaeffer, A., Waley, S. G., and Auld, D. S. (1986) Changes in the coordination geometry of the active-site metal during catalysis of benzylpenicillin hydrolysis by *Bacillus cereus* β-lactamase II. *Biochemistry 25*, 7208–7215.
32. Bicknell, R., and Waley, S. G. (1985) Cryoenzymology of *Bacillus cereus* β-lactamase II. *Biochemistry 24*, 6876–6887.

33. Hu, Z., Peryannan, G., Bennett, B., and Crowder, M. (2008) Role of the Zn-1 and Zn-2 sites in metallo-β-lactamase L1. *J. Am. Chem. Soc. 130*, 14207–14216.
34. Sharma, N., Hu, Z., Crowder, M. W., and Bennett, B. (2008) Conformational changes in the metallo-β-lactamase ImiS during the catalytic reaction: An EPR spectrokinetic study of Co(II)-spin label interactions. *J. Am. Chem. Soc. 130*, 8215–8222.
35. Sharma, N. P., Hajdin, C., Chandrasekar, S., Bennett, B., Yang, K. W., and Crowder, M. W. (2006) Mechanistic Studies on the Mononuclear Zn(II)-Containing Metallo-β-lactamase ImiS from *Aeromonas sobria*. *Biochemistry 45*, 10729–10738.
36. Badarau, A., and Page, M. I. (2006) Enzyme Deactivation Due to Metal-Ion Dissociation during Turnover of the Cobalt-β-Lactamase Catalyzed Hydrolysis of β-Lactams. *Biochemistry 45*, 11012–11020.
37. Bicknell, R., Knott-Hunziker, V., and Waley, S. G. (1983) The pH-dependence of class B and C β-lactamases. *Biochem. J. 213*, 61–66.
38. Hawk, M. J., Breece, R. M., Hajdin, C. E., Bender, K. M., Hu, Z., Costello, A. L., Bennett, B., Tierney, D. L., and Crowder, M. W. (2009) Differential binding of Co(II) and Zn(II) to metallo-β-lactamase Bla2 from *Bacillus anthracis*. *J. Am. Chem. Soc. 131*, 10753–10762.
39. Hernandez, V. M., Kiefer, M., Heinz, U., Soto, R. P., Meyer-Klaucke, W., Nolting, H. F., Zeppezauer, M., Galleni, M., Frere, J. M., Rossolini, G. M., Amicosante, G., and Adolph, H. W. (2000) Kinetic and spectroscopic characterization of native and metal-substituted β-lactamase from *Aeromonas hydrophila* AE036. *FEBS Lett. 467*, 221–225.
40. Yang, Y., Rasmussen, B. A., and Bush, K. (1992) Biochemical characterization of the metallo-β-lactamase CcrA from *Bacteroides fragilis* TAL3636. *Antimicrob. Agents Chemother. 36*, 1155–1157.
41. Paul-Soto, R., Bauer, R., Frere, J. M., Galleni, M., Meyer-Klaucke, W., Nolting, H., Rossolini, G. M., de Seny, D., Hernandez-Valladares, M., Zeppezauer, M., and Adolph, H. W. (1999) Mono- and binuclear Zn^{2+}-β-lactamase. Role of the conserved cysteine in the catalytic mechanism. *J. Biol. Chem. 274*, 13242–13249.
42. Carfi, A., Duee, E., Galleni, M., Frere, J. M., and Dideberg, O. (1998) 1.85 Å resolution structure of the Zn(II) β-lactamase from *Bacillus cereus*. *Acta Crystallogr. D54*, 313–323.
43. Leslie, A. G. W. (1992) Recent changes to the MOSFLM package for processing film and image data. *Joint CCP4 ESF-EADBM Newsletter on Protein Crystallogr 26*, 27–33.
44. Evans, P. R. (1997) Scala. *Joint CCP4 and ESF-EACBM Newsletter 33*, 22–24.
45. Collaborative Computational Project Number 4 (1994) The CCP4 suite: Programs for protein crystallography. *Acta Crystallogr. D50*, 760–763.
46. Navaza, J. (1994) AMoRe: An automated package for molecular replacement. *Acta Crystallogr. D55*, 247–255.
47. Murshudov, G. N., Vagin, A. A., and Dodson, E. J. (1997) Refinement of macromolecular structures by the maximum-likelihood method. *Acta Crystallogr. D53*, 240–255.
48. Emsley, P., Lohkamp, B., Scott, W. G., and Cowtan, K. (2010) Features and development of Coot. *Acta Crystallogr. D66*, 486–501.
49. Laskowski, R. A., Mac Arthur, M. W., Moss, D. S., and Thornton, J. M. (1993) PROCHECK: A program to check the stereochemical quality of protein structures. *J. Appl. Crystallogr. 26*, 283–291.
50. Vaguine, A. A., Richelle, J., and Wodak, S. J. (1999) SFCHECK: A unified set of procedures for evaluating the quality of macromolecular structure-factor data and their agreement with the atomic model. *Acta Crystallogr. D55*, 191–205.
51. DeLano, W. L. (2002) The PyMOL Molecular Graphics System, DeLano Scientific, San Carlos, CA.
52. Garcia-Saez, I., Docquier, J. D., Rossolini, G. M., and Dideberg, O. (2008) The three-dimensional structure of VIM-2, a Zn-β-lactamase from *Pseudomonas aeruginosa*, in its reduced and oxidised form. *J. Mol. Biol. 375*, 604–611.
53. Ullah, J. H., Walsh, T. R., Taylor, I. A., Emery, D. C., Verma, C. S., Gamblin, S. J., and Spencer, J. (1998) The crystal strucuture of the L1 metallo-β-lactamase from *Stenotrophomonas maltophilia* at 1.7 Å resolution. *J. Mol. Biol. 284*, 125–136.
54. Tomatis, P. E., Fabiane, S. M., Simona, F., Carloni, P., Sutton, B. J., and Vila, A. J. (2008) Adaptive protein evolution grants organismal fitness by improving catalysis and flexibility. *Proc. Natl. Acad. Sci. U.S.A. 105*, 20605–20610.
55. Rasia, R. M., and Vila, A. J. (2004) Structural determinants of substrate binding to *Bacillus cereus* metallo-β-lactamase. *J. Biol. Chem. 279*, 26046–26051.
56. Chantalat, L., Duee, E., Galleni, M., Frere, J. M., and Dideberg, O. (2000) Structural effects of the active site mutation cysteine to serine in *Bacillus cereus* zinc-β-lactamase. *Protein Sci. 9*, 1402–1406.
57. González, J. M., Medrano Martin, F. J., Costello, A. L., Tierney, D. L., and Vila, A. J. (2007) The Zn2 Position in Metallo-β-lactamases Is Critical for Activity: A Study on Chimeric Metal Sites on a Conserved Protein Scaffold. *J. Mol. Biol. 373*, 1141–1156.
58. Llarrull, L. I., Fabiane, S. M., Kowalski, J. M., Bennett, B., Sutton, B. J., and Vila, A. J. (2007) Asp-120 Locates Zn2 for Optimal Metallo-β-lactamase Activity. *J. Biol. Chem. 282*, 18276–18285.
59. Garau, G., Di Guilmi, A. M., and Hall, B. G. (2005) Structure-based phylogeny of the metallo-β-lactamases. *Antimicrob. Agents Chemother. 49*, 2778–2784.
60. Garcia-Saez, I., Hopkins, J., Papamicael, C., Franceschini, N., Amicosante, G., Rossolini, G. M., Galleni, M., Frere, J. M., and Dideberg, O. (2003) The 1.5-Å structure of *Chryseobacterium meningosepticum* zinc β-lactamase in complex with the inhibitor, D-captopril. *J. Biol. Chem. 278*, 23868–23873.
61. Bebrone, C., Anne, C., De Vriendt, K., Devreese, B., Rossolini, G. M., van Beeumen, J., Frere, J. M., and Galleni, M. (2005) Dramatic broadening of the substrate profile of the *Aeromonas hydrophila* CphA metallo-β-lactamase by site-directed mutagenesis. *J. Biol. Chem. 280*, 28195–28202.
62. Oelschlaeger, P., Mayo, S. L., and Pleiss, J. (2005) Impact of remote mutations on metallo-β-lactamase substrate specificity: Implications for the evolution of antibiotic resistance. *Protein Sci. 14*, 765–774.
63. Davies, A. M., Rasia, R. M., Vila, A. J., Sutton, B. J., and Fabiane, S. M. (2005) Effect of pH on the active site of an Arg121Cys mutant of the metallo-β-lactamase from *Bacillus cereus*: Implications for the enzyme mechanism. *Biochemistry 44*, 4841–4849.
64. Lindskog, S. (1966) Interaction of Cobalt(II) Carbonic Anhydrase with Anions. *Biochemistry 5*, 2641–2646.
65. Ciszak, E., and Smith, G. D. (1994) Crystallographic Evidence for Dual Coordination Around Zinc in the T_3R_3 Human Insulin Hexamer. *Biochemistry 33*, 1512–1517.
66. Kremer-Aach, A., Klaui, W., Bell, R., Strerath, A., Wunderlich, H., and Mootz, D. (1997) Cobalt as a Probe for Zinc in Metalloenzyme Model Compounds? A Comparison of Spectroscopic Features and Coordination Geometry of Four- and Five-Coordinate Complexes. Crystal and Molecular Structures of [Co(η(3)-Tp(Ph))(η(2)-Tp(Ph))], [(η(3)-Tp(Ph))Zn(anthranilate)], and [(η(3)-Tp(Ph))M(η(2)-acac)] (Tp(Ph) = Hydrotris(3-phenylpyrazol-1-yl)borate, acac = Pentane-2,4-dionate, and M = Zn, Co). *Inorg. Chem. 36*, 1552–1563.
67. Kleifeld, O., Rulisek, L., Bogin, O., Frenkel, A., Havlas, Z., Burstein, Y., and Sagi, I. (2004) Higher metal-ligand coordination in the catalytic site of cobalt-substituted *Thermoanaerobacter brockii* alcohol dehydrogenase lowers the barrier for enzyme catalysis. *Biochemistry 43*, 7151–7161.
68. Badarau, A., Damblon, C., and Page, M. I. (2007) The activity of the dinuclear cobalt-β-lactamase from *Bacillus cereus* in catalysing the hydrolysis of β-lactams. *Biochem. J. 401*, 197–203.
69. Moran-Barrio, J., González, J. M., Lisa, M. N., Costello, A. L., Peraro, M. D., Carloni, P., Bennett, B., Tierney, D. L., Limansky, A. S., Viale, A. M., and Vila, A. J. (2007) The Metallo-β-lactamase GOB Is a Mono-Zn(II) Enzyme with a Novel Active Site. *J. Biol. Chem. 282*, 18286–18293.
70. Cotton, F. A., and Wilkinson, G. (1988) Advanced Inorganic Chemistry: A Comprehensive Text, 5th ed., John Wiley & Sons, New York.
71. Bauer, R., Limkilde, P., and Johansen, J. T. (1976) Low and High pH Form of Cadmium Carbonic-Anhydrase Determined by Nuclear-Quadrupole Interaction. *Biochemistry 15*, 334–342.
72. Holland, D. R., Hausrath, A. C., Juers, D., and Matthews, B. W. (1995) Structural analysis of zinc substitutions in the active site of thermolysin. *Protein Sci. 4*, 1955–1965.
73. Breece, R. M., Hu, Z., Bennett, B., Crowder, M. W., and Tierney, D. L. (2009) Motion of the zinc ions in catalysis by a dizinc metallo-β-lactamase. *J. Am. Chem. Soc. 131*, 11642–11643.
74. Oelschlaeger, P., Schmid, R. D., and Pleiss, J. (2003) Insight into the mechanism of the IMP-1 metallo-β-lactamase by molecular dynamics simulations. *Protein Eng. 16*, 341–350.